Nano-electrochemistry & Nano-photochemistry
https://www.sciltp.com/journals/nenp

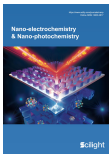

Review

Photo-Biofuel Cell-Based Self-Powered Sensors for Food Safety

Linyun Zhang, Jiaying Bei, Cao Li and Xin Luo *

Key Laboratory of Fermentation Engineering (Ministry of Education), Cooperative Innovation Center of Industrial Fermentation (Ministry of Education & Hubei Province), National "111" Center for Cellular Regulation and Molecular Pharmaceutics, School of Life and Health Sciences, Hubei University of Technology, Wuhan 430068, China
* Correspondence: xluo@hbut.edu.cn

How To Cite: Zhang, L.; Bei, J.; Li, C.; et al. Photo-Biofuel Cell-Based Self-Powered Sensors for Food Safety. *Nano-electrochemistry & Nano-photochemistry* **2026**, *2*(1), 2. https://doi.org/10.53941/nenp.2026.100002

Received: 22 December 2025
Revised: 27 January 2026
Accepted: 28 January 2026
Published: 5 February 2026

Abstract: Photo-biofuel-cell (PBFC) self-powered sensors are emerging as effective tools for food safety analysis because light-driven charge generation can be directly coupled with redox catalysis to produce bias-free signals with inherent amplification in complex matrices. Unlike photoelectrochemical sensors that commonly depend on external biasing or sacrificial reagents and biofuel cell sensors restricted by limited driving force and catalyst instability, PBFCs function as closed energy signal systems in which photovoltage and interfacial reaction pathways jointly govern signal output. This review consolidates recent progress by relating photocarrier behavior, interfacial field regulation, and cathodic charge utilization to analytical sensitivity, operational stability, and matrix tolerance. Material and interface strategies across photoanodes, photocathodes, and recognition layers are examined, including band structure modulation, heterojunction construction, conductive architectures, and interface gating for controlled charge transfer upon target binding. Representative applications involving antibiotics, pesticides, heavy metals, and toxins are discussed with attention to dual photoelectrode operation, microfluidic regulation, and ratiometric or multiplex readouts. These developments indicate that PBFCs are advancing toward reliable on-site sensing in real food matrices.

Keywords: photo-biofuel cells; self-powered sensors; photoelectrode; food safety

1. Introduction

Food contamination remains a long-standing concern for public health and for maintaining confidence in increasingly intricate supply systems [1–3]. As a result, there is growing interest in portable analytical methods that can evaluate chemical residues, biological risks, and freshness directly within real samples, where elevated salinity, shifting pH, and high organic content frequently compromise signal stability [4–6]. Although electrochemical and photoelectrochemical approaches offer strong sensitivity in controlled experiments, their broader use in decentralized and prolonged monitoring is often constrained by the need for external power, wired instrumentation, and reagent-dependent workflows that are difficult to sustain outside laboratory settings [7–9].

Self-powered electrochemical sensors are attracting attention as a field-oriented alternative [10–12]. By harvesting locally available energy and converting it into an immediately readable electrical output, these devices offer a route to in situ measurements that are less dependent on auxiliary hardware and more compatible with decentralized, data-enabled food-monitoring workflows [13–15]. Early biofuel-cell sensors demonstrated bias-free detection using enzymatic or microbial oxidation of fuels such as glucose and lactate, but practical translation is frequently constrained by limited redox driving force, slow interfacial kinetics, and biocatalyst instability [16–18]. Photo-biofuel cells (PBFCs) represent a distinct evolution in which light harvesting at a semiconductor

Copyright: © 2026 by the authors. This is an open access article under the terms and conditions of the Creative Commons Attribution (CC BY) license (https://creativecommons.org/licenses/by/4.0/).
Publisher's Note: Scilight stays neutral with regard to jurisdictional claims in published maps and institutional affiliations.

photoelectrode is coupled to catalytic redox turnover at the counter electrode, enabling photovoltage-assisted, bias-free signal generation with improved tunability and matrix tolerance [19–21]. By integrating semiconductor energetics with recognition elements, including aptamers, enzymes, and molecularly imprinted polymers, PBFCs can translate molecular interactions into regulated charge-transfer modulation while operating as a self-contained energy-signal circuit [22,23].

Although notable advances have been achieved, the progression of photo-biofuel cells from laboratory studies to practical food monitoring remains constrained by several coupled factors. Key limitations include inadequate long-term stability of photoelectrodes and biointerfaces, inefficient conversion of harvested energy into detectable signals under transport and contamination pressure, and insufficient system integration that compromises reproducibility in non-controlled settings. This article presents the fundamental operating concepts of PBFCs, assesses material and interface design spanning photoanodes, photocathodes, and recognition layers, and reviews representative food safety applications (Figure 1).

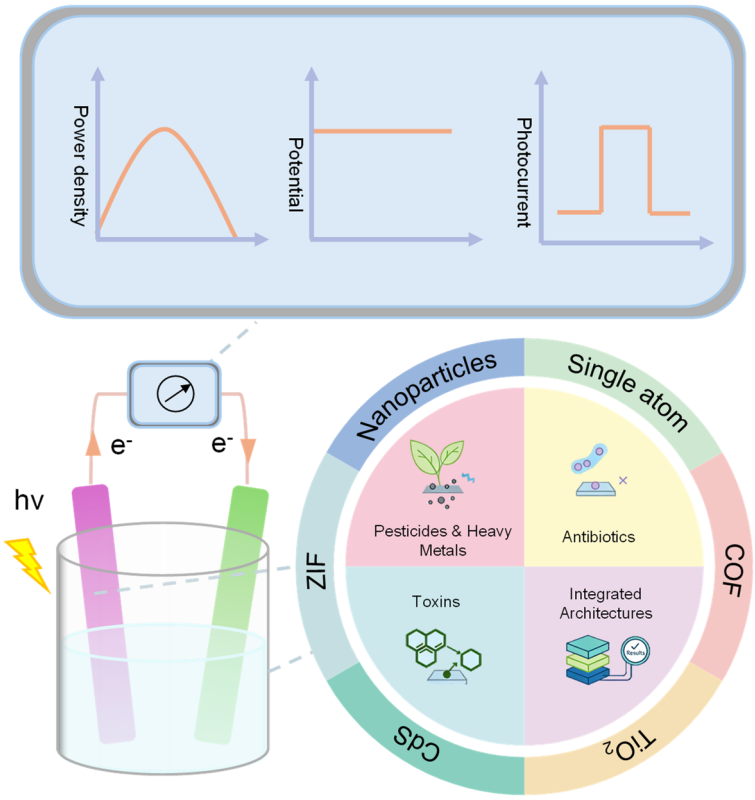

Figure 1. Schematic illustration of the PBFC-based sensing platform for food safety.

2. Fundamental Principles

2.1. Distinction from PEC, BFC, and PBFC Platforms

PBFCs bridge photoelectrochemical systems and biofuel cells, but they operate through an independent circuit, in which energy conversion and signal output are intrinsically interrelated [24]. Photoelectrochemical sensing generates signals through photogenerated charge carriers on the semiconductor electrodes. However, for long-term operation, external bias or sacrificial reagents are usually required to maintain the directional charge flow and the continuous redox reaction process. BFC sensors can generate electrical energy output through the biochemical fuel conversion process, without the need for an external bias voltage. However, their performance is limited by factors such as the weak redox driving force, the slow electron transfer kinetics, and the sensitivity of the biological catalyst to changes in pH value, temperature, and ionic strength. These limitations generally result in low output voltages, frequently below 0.4 V, together with reduced operational stability in chemically complex food matrices [25,26].

PBFCs mitigate both limitations by coupling light harvesting with catalytic redox chemistry so that photovoltage supplements biochemical driving force and accelerates interfacial charge transfer without external bias. Under illumination, quasi-Fermi-level splitting at the photoelectrode provides an additional potential window beyond enzymatic catalysis, enabling faster substrate oxidation and more efficient counter-electrode reactions. As a result, PBFCs commonly deliver open-circuit voltages of about 0.5–0.8 V and photocurrent densities in the

hundreds of μA cm^{-2}, consistent with improved carrier separation and interfacial kinetics. Beyond energetics, PBFCs benefit from a two-electrode layout that eliminates PEC bias circuits and supports integration into flexible substrates, paper-based formats, and microfluidic devices. In many designs, the target analyte (for example, saccharides, pesticides, or toxins) participates directly in one half-reaction, coupling energy conversion with analyte transformation to enable quantification and, in some cases, partial mitigation.

A closely related step toward autonomy is dual-photoelectrode coupling, where an n-type photoanode and a p-type photocathode create an internal electric field that drives charge transport without external bias and spatially separates oxidation from reduction reactions [27]. Interfacial-field engineering provides a materials-level handle for this autonomy; for example, a $BiVO_4$/MXene Schottky junction establishes a built-in field that promotes electron extraction and suppresses recombination [28]. To improve charge utilization, semiconductor-catalyst coupling can further create compensated redox pathways. A metal-halide perovskite with a CoNiFe layered hydroxide cocatalyst achieved high photocurrent and Faradaic efficiency for gluconic-acid formation, illustrating how catalytic selectivity and photovoltage can be co-optimized within an integrated energy-conversion scheme (Figure 2a) [29]. Related interface layers can simultaneously tune band energetics and adsorption selectivity; in $BiVO_4$/BN/FeNiOOH (Figure 2b), BN facilitated hole extraction while modulating interfacial energetics and *OOH adsorption, enabling sustained operation through coupled field and catalytic regulation [30].

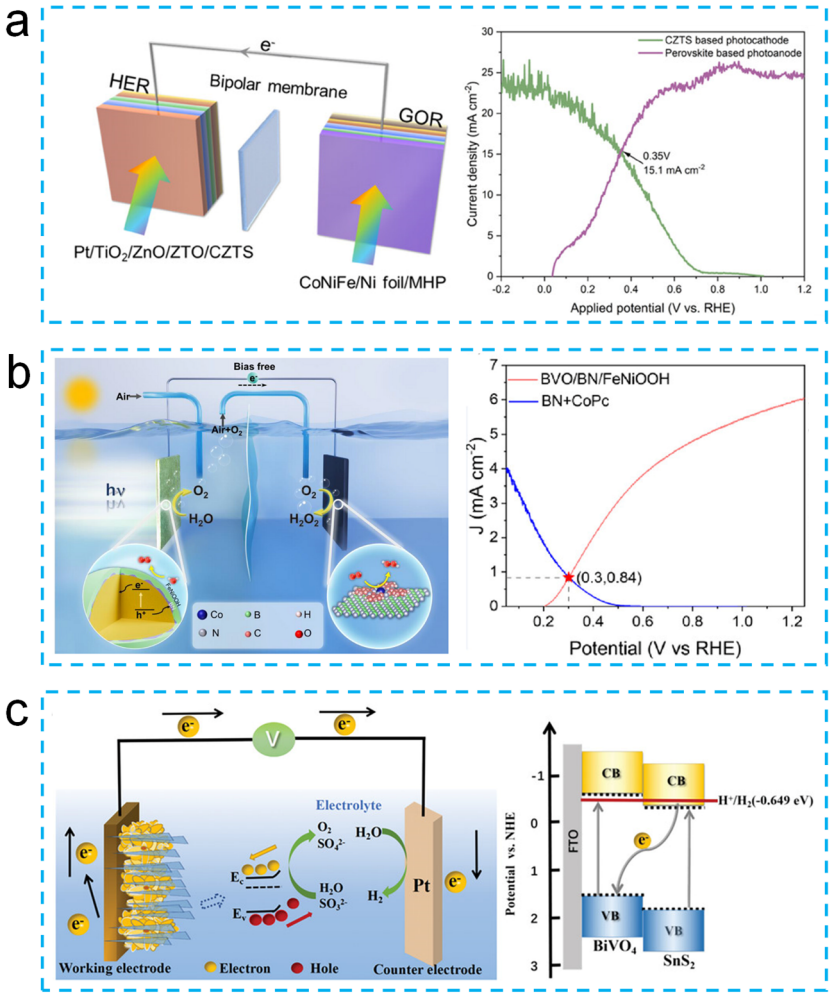

Figure 2. (**a**) Schematic illustration of the PEC H_2-GOR system, Reprinted with permission from Ref. [29]. Copyright 2025, Wiley-VCH. (**b**) Schematic of photoelectrocatalytic system with BVO_4/BN/FeNiOOH photoanode and the CoPc + BN cathode. Reprinted with permission from Ref. [30]. Copyright 2025, Wiley-VCH. (**c**) Schematic illustration of SnS_2/$BiVO_4$ photoanode. Reprinted with permission from Ref. [31]. Copyright 2023, Wiley-VCH.

Coupling geometry with electrostatics can reinforce self-powered response at the device level. A hollow In_2S_3@$CdIn_2S_4$ photoanode paired with a $CuInS_2$ photocathode benefited from enhanced photon capture and inter-electrode Coulombic effects that facilitated carrier migration, enhancing output [32]. Triboelectric and piezoelectric nanogenerators have been demonstrated as viable power sources for cardiac pacemakers, with

reported open-circuit voltages reaching 65.2 V, indicating the potential for practical application [33]. Therefore, self-powered systems highlight the benefit of unifying energy harvesting with functional signal output.

Together, these advances define PBFCs as unified energy-signal circuits in which semiconductor photogeneration and coupled redox chemistry produce autonomous sensing outputs under illumination. This intrinsic co-generation of power and analytical signal constitutes the key mechanistic distinction from conventional PEC and BFC platforms, and establishes the foundation for bias-free, high-fidelity, and energy-autonomous sensing in complex food matrices.

2.2. Working Mechanism

The operation of PBFCs relies on coordinated coupling of light harvesting, semiconductor charge management, interfacial electric-field regulation, and catalytic redox conversion. These processes determine how photons are converted into free carriers, how carriers are extracted across semiconductor-electrolyte interfaces, and how they ultimately drive analyte-responsive electrochemical reactions that enable autonomous sensing [34,35].

2.2.1. Photogenerated Carrier Dynamics

In PBFCs, the sensing signal originates from the generation and separation of photogenerated carriers within semiconductor photoelectrodes [36,37]. Upon illumination, electrons are promoted from the valence band to the conduction band to form electron-hole pairs, and their separation under built-in fields establishes the photovoltage or photocurrent that powers downstream redox reactions [38]. Whether these nonequilibrium carriers participate effectively in analyte-linked processes depends on band structure, the distribution and energetics of trap states, and interfacial fields that facilitate carrier extraction [39]. Trap-assisted recombination at bulk or surface defects is a dominant loss pathway and becomes more pronounced in food matrices, where ions, organic residues, and pH fluctuations continuously perturb surface states. In practice, stable readout hinges on getting the semiconductor "details" right: tuning composition, steering facet exposure, and passivating reactive sites to curb recombination, keep carriers mobile, and prevent signal drift in real samples [40].

2.2.2. Heterojunction and Interface Engineering

PBFC electrodes frequently employ semiconductor heterojunctions to strengthen charge separation without weakening redox activity. When semiconductors with different Fermi levels are coupled, charge redistribution at the interface produces an internal electric field that drives electrons and holes into distinct regions [41]. In standard junctions, this separation follows staggered band edges, whereas Z scheme arrangements favor recombination of low-energy carriers while retaining strong oxidation and reduction capability. The SnS_2/$BiVO_4$ pairing illustrates this behavior, with suitable energy alignment and interfacial coupling enabling efficient carrier extraction and controlled oxygen reduction (Figure 2c) [31,42]. Further regulation is achieved through structural and optical design. In t-Se/InSe systems, photocurrent direction depends on excitation wavelength as different redox routes dominate under varying illumination [43]. Hierarchical In_2O_3 nanosheets shorten transport pathways and expose more reactive sites, while SiC/Au plasmonic hybrids intensify local electromagnetic fields that support interfacial separation. Layered $MnPSe_3$ adds internal interlayer fields that broaden absorption into the visible and near infrared range [44,45]. Collectively, these cases show that PBFC performance improves through combined tuning of band alignment, interface chemistry, and optical or structural features that increase carrier generation, separation, and effective use.

2.2.3. Cathodic Redox Processes and Charge Utilization

Cathode electrons are a crucial factor in PBFCs, as it determines the achievable current output, guide the reduction reaction pathway, and ensure stability during long-term operation. Electron-uptake kinetics and charge-transfer pathways depend on catalyst electronic structure, active-site distribution, and chemical resilience. Heterostructured photocathodes such as In_2Te_3/Se enable rapid electron injection via aligned energetics [46–50].

Dual-photoelectrode configurations further elevate charge utilization by leveraging the Fermi-level difference between photoanode and photocathode to drive spontaneous, bias-free carrier migration. Systems such as WO_3@CdS paired with Co-$CuInS_2$, or SnS_2/In_2S_3 combined with $CuInS_2$, illustrate how inter-electrode energetic matching stabilizes separation and supports sensitive analyte readout [51–53]. Enzyme-based cathodes (for example, BOD) can also be used to improve reduction kinetics under benign conditions [54]. More recently, photo-coupled ion transfer concepts indicate that long-lived photocarriers can drive ion migration at donor-acceptor interfaces, broadening PBFC function beyond classical electron-transfer schemes (Figure 3) [55].

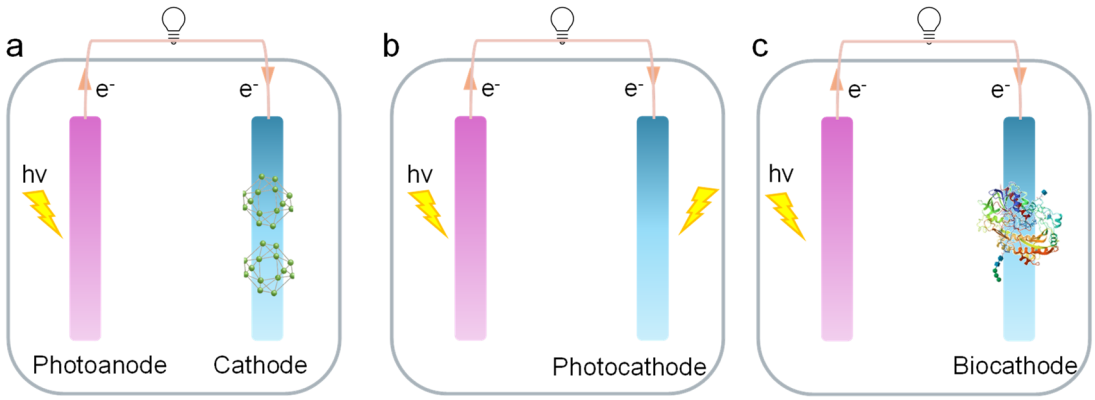

Figure 3. Scheme of self-powered systems with photoanode powered by (**a**) cathode, (**b**) photocathode, and (**c**) biocathode.

Beyond sensing-oriented configurations, PBFC concepts have been extended toward broader photoelectrochemical energy-signal coupling. TN-COF@CNT hybrid electrodes, for example, illustrate how donor-acceptor covalent frameworks integrated with conductive backbones can sustain long-lived charge separation and support photo-coupled ion-transfer processes [56]. These results reinforce a unified mechanistic picture: efficient PBFC operation depends on coordinated control of light absorption, carrier dynamics, band alignment, interfacial fields, and catalytic redox pathways. When semiconductor energetics and catalytic processes are matched across the device, PBFCs sustain directional charge flow and analyte-dependent reactions without external power, providing a robust basis for autonomous monitoring in complex food and environmental matrices.

3. Materials and Interface Design

3.1. Photoanodes and Band Engineering

The analytical performance of PBFC-based self-powered sensors arises from the coordinated function of three constituents: light-collecting photoanodes, electron-consuming catalytic cathodes, and target-responsive recognition interfaces. Materials selection and interfacial construction together set the ceiling for photon-to-electrical conversion, govern output stability in matrix-rich samples, and define the fidelity with which binding events are converted into measurable electrical modulation [57]. The electronic structure of the photoelectrode defines the underlying energy landscape, regulating light absorption, the formation of photogenerated carriers, the directionality of charge migration, and their effective participation in analyte-related redox reactions. Semiconductor materials, including TiO_2, $BiVO_4$, CdS, and g-C_3N_4, are therefore commonly employed owing to their suitable band-edge positions and chemical robustness [58]. In practical operation, however, their performance is often constrained by limited visible-light utilization, short carrier transport lengths, and rapid recombination of photogenerated charges.

Energy-band modulation provides the fundamental constraint for design at this level by defining the thermodynamic space within which photogenerated carriers can separate and migrate. The SnS_2/$BiVO_4$ photoanode was reported to sustain current densities of several hundred microamperes per square centimeter while delivering photovoltages close to 0.8 V [31]. However, higher voltage does not necessarily translate into superior reaction outcomes. This interplay is illustrated by surface-modified $BiVO_4$/$BiPO_4$, where preferential carbonate adsorption alters intermediate binding relative to peroxide species, steering the oxygen reduction reaction toward the two-electron pathway [59].

Exclusive reliance on static band-structure tuning rarely suffices to govern photoelectrochemical behavior under realistic operating conditions. In contrast, a stable interfacial field supports continued carrier separation and preserves transport directionality as the chemical environment changes. This principle is evident in compositionally graded interfaces, including ZnO/$ZnAl_2O_4$ and doped hematite structures, where internal fields remain effective in guiding carrier migration even under non-ideal conditions [60]. The internal potentials established at these interfaces can still promote carrier migration when electrolyte chemistry is disturbed. In ZnO/$ZnAl_2O_4$ from ZnAl-LDH, the enhanced light response is consistent with the improved cyclic stability, which is consistent with the experimental evidence that the field adjustment interface is more able to withstand long-term operation despite the changing surface state. The influence of the interface field also extends to the catalytic performance. In the $BiVO_4$/CoFe-LDH composition, the coordination between the redox energy and the charge transmission path supports the allyl C-H oxidation reaction, and its selectivity is close to 97%, indicating that the

reaction kinetics and field-oriented carrier transmission can be jointly promoted on the photoanode, without competing with each other for optimization [61]. The third layer originates from exciton regulation and the dis-domainization of molecular-scale charge, which becomes crucial in materials with strong Coulomb bonds. In this system, exciton dissociation rather than free carrier migration is often the main bottleneck [62]. Donor-receptor covalent organic frameworks such as TAT-COF and $CsPbBr_3$@COF-V introduce extended π-off-domain and directional electron coupling, thus reducing the exciton binding energy and guiding the charge to separate along the preferred channel (Figure 4a) [63,64]. The covalent organic framework integrates dense π-conjugation with the redox activity of metal centers, enabling nanomolar-level detection of nitrogen dioxide. This result demonstrates that exciton-landscape engineering introduces an adjustable design dimension that remains largely inaccessible to conventional metal-oxide materials. These frameworks transformed by molecular engineering technology can extend the life of carriers and can programmably control the conversion process between photocarriers and free carriers.

On the medium scale and device scale, the extended conduction network ensures that the locally generated carriers can pass through the electrode without compounding or being captured, which becomes crucial in the case of ion disturbance, pH changes, and organic dirt common in PBFC operation [65–68]. Due to its high carrier mobility and adjustable surface end base, MXenes can form a multi-domain conductive framework and can withstand strain and chemical fluctuations. For example, structures such as Co-PBA@MXene and Cu-TCPP/$BiVO_4$ show that the conductive dimension can stabilize charge transmission during long-term operation, and can maintain a 95% optical current retention rate even in systems rich in defects or catalytic activity (Figure 4b) [69,70]. In short, these results show that the conduction continuity at the device level provides a basis for linking local optical physical properties with macroscopic output stability.

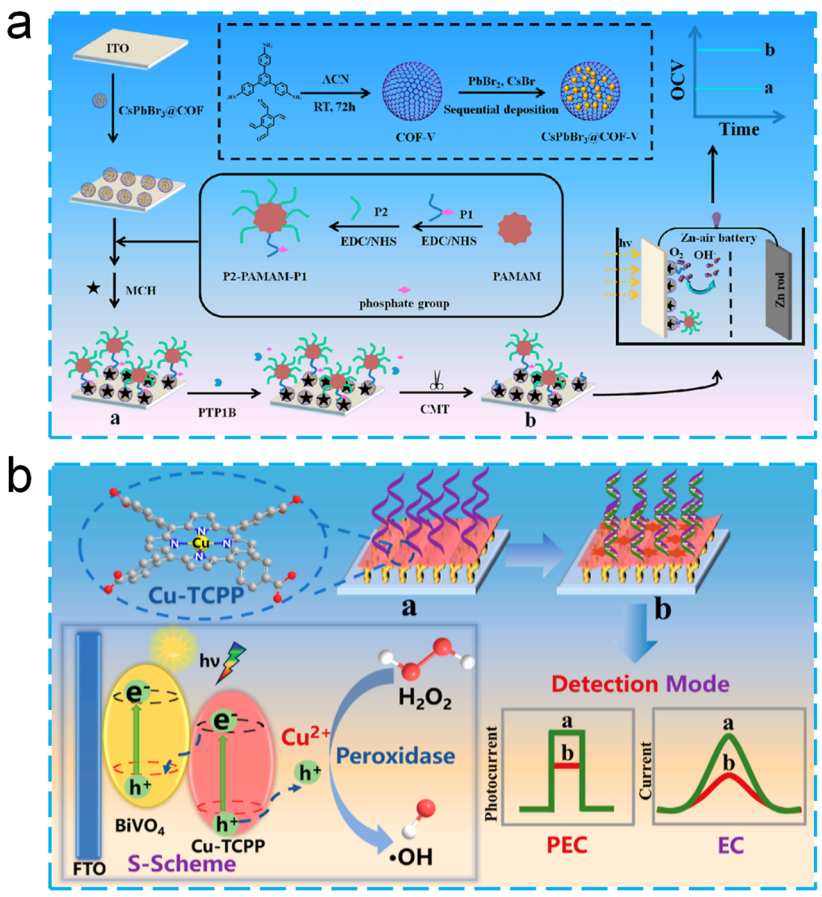

Figure 4. (**a**) Schematic illustration of the zinc-air battery-assisted PEC sensing, Reprinted with permission from Ref. [64]. Copyright 2022, American Chemical Society. (**b**) Schematic illustration of dual-mode sensing. Reprinted with permission from Ref. [70]. Copyright 2025, American Chemical Society.

Overall, high-performance PBFC photoanodes emerge not from isolated improvements in visible-light harvesting, but from hierarchical integration of band geometry, interfacial field architectures, exciton-dissociation pathways, and conduction-network continuity. Through such multiscale coordination, photoanodes evolve from

simple absorbers into coherent energy–signal transducers capable of delivering strong, stable, and chemically selective outputs in interference-prone food-safety environments.

3.2. Cathodes and Photocathodic Interfaces

The photocathode defines the terminal electron-consumption pathway in PBFCs and therefore governs photocurrent magnitude, ORR selectivity, and operational stability [71]. Because PBFCs operate without external bias and often under low-oxygen, chemically heterogeneous food matrices, photocathodic design must simultaneously address oxygen availability, interfacial charge-transfer continuity, active-site chemistry, and long-range electron transport.

A first practical constraint is oxygen accessibility. In many PBFC settings, early-stage ORR performance is limited more by local O_2 transport than by intrinsic catalytic activity [72]. Accordingly, solid-liquid-air triphase interfaces are frequently introduced to buffer O_2 concentration near the cathode and to stabilize electron utilization, establishing a transport-controlled baseline for reliable photocathodic operation. Beyond oxygen supply, heterostructure-mediated carrier transfer is central to reductive stability. Band-aligned junctions, exemplified by Cu_2O/CuO systems protected by thin conductive coatings, maintain continuous electron flow while suppressing photocorrosion under illumination [73]. This design logic parallels the band and field co-regulation strategies used for photoanodes, but here it is leveraged to preserve cathodic integrity and sustain ORR turnover under chemically fluctuating conditions.

At the electronic-structure scale, single-atom catalysts provide a highly precise route for steering reaction pathways through their well-defined coordination motifs [74]. When analogous atomic sites are incorporated on both electrodes, their role expands from regulating local reaction steps to shaping charge distribution and transport throughout the PBFC, thereby enhancing electron utilization at the device level (Figure 5) [75]. Modifying the type and exposure of crystal facets alters surface electronic states and oxygen adsorption geometries, which can lower reaction barriers [76]. In practical application, sustaining continuous electron flow is equally important, since fluctuations (such as ionic strength, pH, and surface fouling) can readily interrupt conductive pathways [77,78]. To address these challenges, MXene-based materials have gained increasing attention due to their high catalytic activity and excellent mechanical and chemical stability.

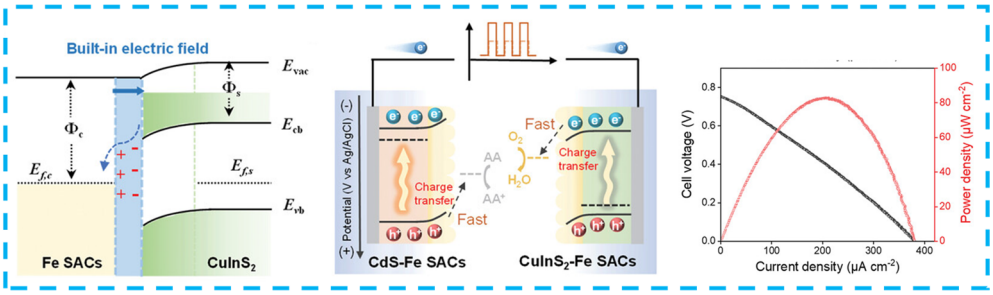

Figure 5. Schematic illustration of the charge transfer process for CdS-CuInS$_2$-Fe SACs-based PEC fuel cells. Reprinted with permission from Ref. [75]. Copyright 2023, Wiley-VCH

Taken together, high-performance photocathodes emerge from the coordinated regulation of oxygen delivery, heterostructure energetics, atomic-site chemistry, facet-level microenvironments, and multidomain conduction continuity [79]. This multiscale integration transforms photocathodes from passive electron sinks into actively engineered redox interfaces capable of sustaining stable, high ORR in complex food-matrix conditions.

3.3. Recognition Interfaces

The recognition interface determines how molecular binding events are converted into measurable electronic outputs in PBFC-based sensors. Rather than serving as a passive probe-immobilization layer, it operates as an electronically coupled interfacial domain that modulates carrier extraction, local fields, and interfacial redox selectivity. Because PBFCs are often deployed in chemically heterogeneous food matrices, recognition layers are increasingly engineered as functional regulators of charge transfer, not simply as molecular "labels" attached to an electrode surface.

A first design requirement is stable and electronically coherent anchoring, which secures probe orientation while suppressing nonspecific adsorption. Chemically bonded two-dimensional scaffolds (e.g., MXenes), together with self-assembled monolayers and zwitterionic antifouling coatings, create ordered adsorption environments that

preserve continuous electron pathways [80]. By stabilizing variations in the interfacial electric field, low-impedance charge transfer can be sustained even as ionic strength and pH in a real sample.

A complementary strategy relies on gating effects arising from conformational change or reaction-driven restructuring at the interface. In this mode, target binding functions not only as a recognition step but also as an active modifier of the local charge-transfer geometry through induced structural rearrangement. Responsive elements such as adaptive molecular switches, DNA-based structural motifs, and enzyme-activated surface reorganization can reshape spatial access, adjust the interfacial electrostatic landscape, or reposition catalytic centers, thereby redirecting carrier pathways and modulating their effective utilization [81,82]. In addition, recognition extends beyond static interfacial binding by incorporating stimulus-responsive components and integrated signal pathways. At the device level, coordinating molecular recognition with semiconductor energy-level alignment and photocathodic processes promotes more balanced charge utilization and supports stable, dependable signal output under realistic operating conditions [83,84].

Overall, PBFC recognition interfaces have progressed from static ligand layers to multifunctional, electronically engaged architectures [85,86]. By embedding molecular recognition within charge-transport and field-modulation frameworks, these interfaces provide the selectivity, drift resistance, and matrix tolerance required for reliable sensing in complex food-safety and environmental applications.

3.4. Integrated Architectures

Integrated PBFC architectures emerge when the photoanode, photocathode, and recognition interface function as coupled elements within a single energetic landscape, rather than as independently optimized modules. In this regime, photonic excitation, carrier transport, redox turnover, and molecular recognition proceed as a coordinated cascade, such that the interfacial response at one component predictably conditions the kinetics and selectivity of the next. The defining feature of an integrated PBFC is therefore the coherence with which photophysical and electrochemical processes are synchronized across the full device.

A primary manifestation of this coherence is directional charge transport becoming a system-level property. When hierarchical sulfide–oxide photoanodes are paired with $CuInS_2$-type photocathodes, complementary band structures establish a continuous potential gradient that channels photogenerated carriers with reduced energetic loss [87]. The resulting stabilization of PEC output and enhancement of cathodic turnover indicate that electrode-to-electrode energetic matching can be more decisive than incremental upgrades to either electrode in isolation. Integration is further extended to the field of conduction design, in which individual photochemical events are mapped to independent reading methods. Dual-mode systems such as Nb_2O_5/CdS-BiOI can produce photoelectric and colorimetric reactions at the same time, so that one signal can confirm another in a chemically complex environment [88]. The design converts a single recognition event into coordinated signal outputs that reinforce one another, improving measurement reliability without adding structural or operational complexity to the device.

At the interface level, local regulation can ensure that the system can maintain stable operation even if the surrounding chemical environment changes. For the surface-treated $BiVO_4$/$BiPO_4$ photoanode, by adjusting the interface energy, priority is given to select specific reaction intermediates, so as to promote oxygen reduction to the bi-electron pathway, thus inhibiting the drift of optical voltage [59]. The integration effect can also be enhanced by limiting the space of those components that are prone to degradation. In the component that combines CdIn2S4/CdS photoanode with NH_2-MIL-125(Ti)@$MAPbI_3$/Au photocathode, the metal organic framework (MOF) matrix protects the calcite material while maintaining electronic continuity, thus achieving guided charge transfer [89]. Dynamic reconfiguration offers a pathway toward PBFC systems that can adapt to changing operating conditions. In TiO_2/$ZnIn_2S_4$-Cu_2O/Cu_3SnS_4 assemblies, enzyme-induced removal of MnO_2 initiates a cascade of optical and catalytic adjustments, resulting in enhanced photocurrent generation without applied bias [90]. PBFC technologies are advancing toward durable, high-precision platforms that can operate reliably in the chemically complex conditions typical of real food-safety assessment.

4. Applications in Food Safety

Combining photoactivated oxidation at the anode with biocatalytic oxygen reduction at the cathode, PBFCs generate stable electrical responses from light under ambient conditions [91]. Their self-sustaining energy supply, modular design, and tolerance to chemically complex food matrices support continuous and spatially distributed monitoring. The next section reviews representative food-safety applications of PBFC-based self-powered sensors, charting their development from single-analyte measurements to multiplex and multi-matrix detection while relating design decisions to operational performance.

4.1. Antibiotic Detection

Antibiotic residues are frequently encountered in foods and water systems, and their large-scale use in livestock and agricultural settings has intensified attention to long-term accumulation and the risk of antimicrobial resistance. Rapid, sensitive, and on-site detection is therefore essential. PBFC-based self-powered sensors provide a compelling route by enabling bias-free operation, high analytical sensitivity, and strong adaptability to chemically complex food matrices.

Early PBFC antibiotic sensors primarily improved photoelectrode energetics through heterojunction and defect engineering. Ferroelectric polarization-assisted $TiO_2/BaTiO_3$ photoanodes with oxygen-vacancy enrichment exemplify this strategy, where defect-induced band modulation and polarization fields jointly promote charge separation (Figure 6a) [92]. Coupled with kanamycin-specific aptamers, this configuration achieves femtomolar-level detection with high recovery in fish and milk samples, illustrating how interfacial band regulation can translate directly into signal gain.

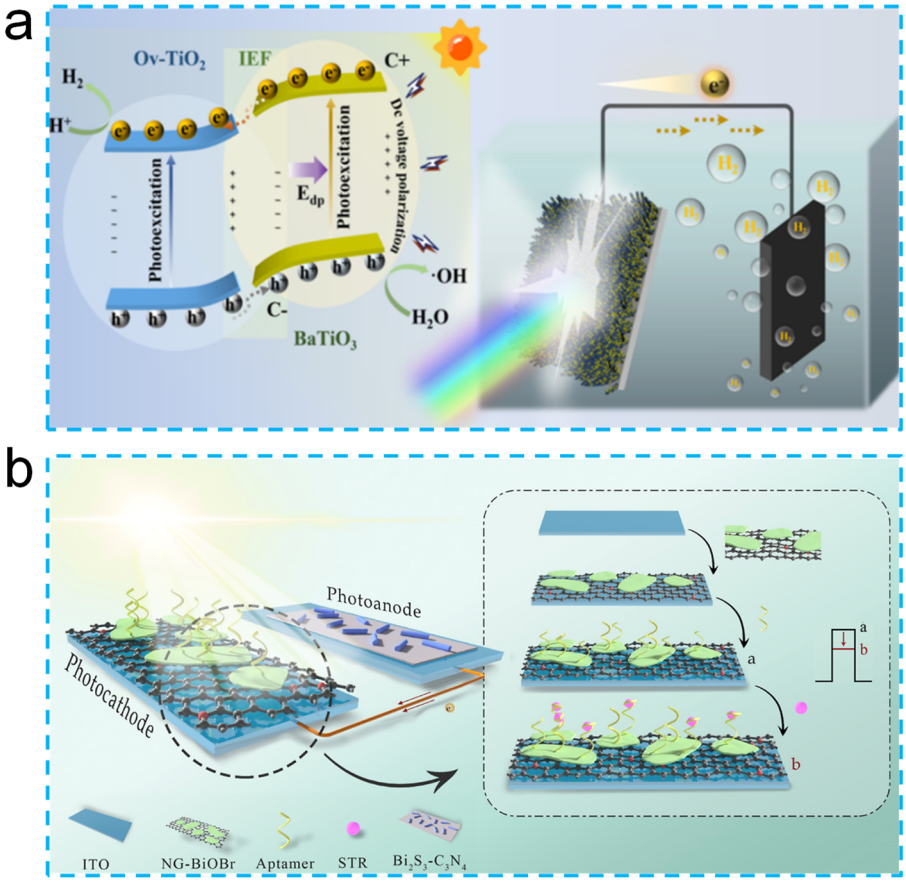

Figure 6. (**a**) Schematic illustration of photoelectric signal enhancement in the Ov-TiO_2/BTO heterojunction. Reprinted with permission from Ref. [92] Copyright, 2025, American Chemical Society. (**b**) Schematic illustration of a Bi_2S_3-C_3N_4-based PEC aptasensor for STR Detection. Reprinted with permission from Ref. [93] Copyright, 2023, American Chemical Society.

More advanced PBFC architectures amplify target-induced modulation by coupling photoanodic and photocathodic processes within dual-photoelectrode platforms. In a representative streptomycin sensor, a Bi_2S_3-C_3N_4 photoanode paired with an N-doped graphene-BiOBr photocathode produced pronounced photocurrent enhancement under zero bias by suppressing recombination and promoting interfacial charge separation, enabling sub-picomolar detection in river water (Figure 6b) [93]. A related design principle was demonstrated using ZnO/ZnS/Ag_2S heterostructured photoanodes combined with Fe-doped $CuBi_2O_4$ photocathodes modified by molecularly imprinted polymers, showing that heterojunction energetics and recognition constraints can be co-integrated to deliver ultralow detection limits with strong matrix tolerance [94]. Microfluidic integration further strengthens PBFC robustness by stabilizing mass transport and enabling localized signal regulation. A microfluidic $SnO_2/CdLa_2S_4$ heterojunction system exploited in situ ion exchange to dynamically modulate band structure and photocurrent output upon kanamycin binding, achieving fg mL^{-1} sensitivity together with high reproducibility and

operational stability [95]. This flow-controlled microenvironment highlights a practical pathway for translating PBFC sensing from static assays to real-sample analysis.

PBFC devices are gradually advancing from single-target analysis toward multiplex and multi-channel sensing formats that offer greater resilience during prolonged operation. One example is a regeneration-free dual-photoelectrode configuration combining a pyurea-COF photocathode with a $BiVO_4$/UiO-66 photoanode, which allows stepwise identification of kanamycin and tobramycin using magnetic-bead logic [96]. By avoiding chemical renewal and surface restructuring, this approach reduces electrode wear and signal cross-talk, enabling stable signal output over extended use. Detection of oxytetracycline further reflects the coupled roles of energy-level control and interface engineering in PBFC systems [97]. Architectures based on ZnO@Co_3O_4 photoanodes paired with Cu_2O photocathodes reach sub-picomolar sensitivity through coordinated heterojunction energetics and restrained interfacial recombination. These results indicate that high sensitivity depends less on light absorption alone and more on balanced regulation of carrier extraction and recombination [42]. PBFC-derived design ideas are being extended toward antifouling and regenerative sensing modes, which support sustained performance in environments with high organic content. Concurrently, PBFC design is expanding toward antifouling and self-renewing sensing strategies to suit environments with high organic content. Photo-renewable ZIF-8 electrodes exhibit illumination-induced self-cleaning, allowing photocurrent recovery after fouling and supporting consistent detection of sulfonamide antibiotics in natural water samples [98].

4.2. Pesticides and Heavy Metals Detection

Pesticides and heavy metals persist as widespread contaminants in food and aquatic systems, where prolonged exposure to trace levels can result in cumulative accumulation and high toxicity [99]. Conventional electrochemical assays often drift in real matrices because surface fouling, ionic-strength fluctuations, and competing redox species distort interfacial charge transfer. PBFC-based self-powered sensors mitigate these constraints by operating without external bias and by using light-driven carrier generation as an intrinsic amplification handle. This handle can be coupled to molecular recognition or to direct analyte-interface interactions, supporting robust on-site monitoring under chemically variable conditions.

For pesticide analysis, one mechanistic route is to stabilize photoelectrode energetics through defect and interface engineering so that photocurrent remains responsive in harsh environments. In atrazine sensing, oxygen-vacancy-enriched $BiVO_4$ photoanodes combined with plasmonic Ag nanoparticles enabled a homogeneous PEC aptasensing configuration with sub-picomolar detection, while preserving signal integrity across broad pH and ionic-strength windows (Figure 7) [100]. This case shows how vacancy-mediated band modulation and plasmon-assisted charge recovery can jointly sustain carrier extraction and protect analytical sensitivity in fluctuating media. A second route is to amplify weak target-induced modulation by coupling photoanodic and photocathodic processes within a dual-photoelectrode PBFC, while embedding selectivity at the interface. For dimethoate, an Ag_2S/SnS_2 photoanode paired with an Fe-doped CBFO photocathode and integrated with molecularly imprinted polymers achieved a sensitive, interference-resistant readout in fruit samples [101]. Here, heterojunction-enabled energy harvesting provides the driving force, whereas imprinting-based recognition constrains the response to the target, yielding a co-designed strategy that improves both sensitivity and matrix tolerance. Beyond probe-dependent schemes, PBFC sensing can also be realized through recognition-free electronic coupling at engineered interfaces, where specificity is encoded in the charge-transfer pathway itself. For chlorpyrifos, an AgBr/Ti_3C_2 MXene Schottky heterojunction leveraged metal-ligand charge transfer between the analyte and Ti sites to induce selective photocurrent quenching, avoiding biological probes while retaining strong recoveries in diverse food matrices [102]. This mechanism highlights a complementary design philosophy in which interfacial electronic structure acts as the selectivity gate.

Alongside organic pesticides, PBFC-inspired designs are extending to heavy-metal ion monitoring using environmentally benign interfaces that support multiplex readout. A metal-free carbon black anchored g-C_3N_4 framework enabled photo-assisted electrochemical detection of Pb^{2+}, Cd^{2+}, and Hg^{2+} with well-resolved, interference-free signals under illumination [103]. By combining the conductivity of carbon black with defect-rich g-C_3N_4 photoactivity, the hybrid interface promotes charge migration and suppresses recombination, yielding stable, distinguishable oxidation peaks for simultaneous quantification in complex aqueous environments. Multifunctional interface development is illustrated by a tetraphenylethylene-derived Dy-MOF, in which one framework enables electrochemical recognition of Cr(VI) together with visible-light-driven transformation to Cr(III) [104]. Ligand-to-metal charge transfer in this material couples analytical response with photocatalytic detoxification, underscoring PBFC-aligned architectures that combine pollutant detection and remediation within a single energy-converting system.

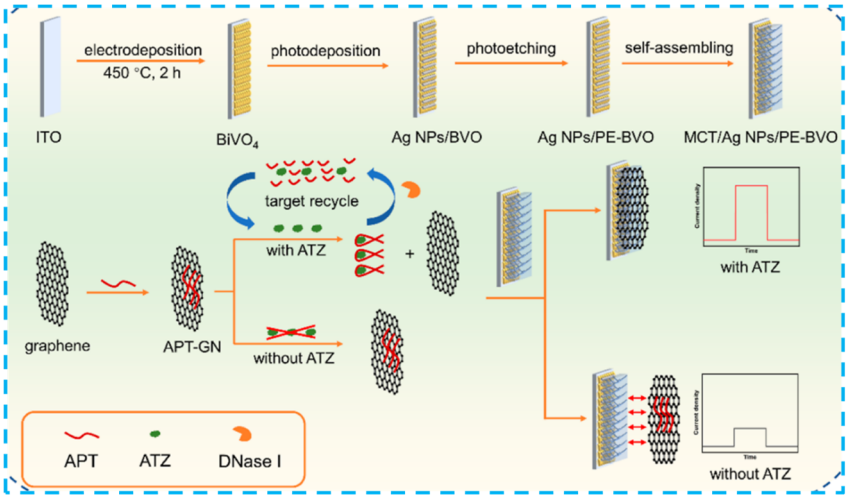

Figure 7. Scheme of the Label-Free PEC Aptasensing. Reprinted with permission from Ref. [100]. Copyright, 2024, American Chemical Society.

Overall, these reports show that PBFC sensors can accommodate a wide range of pesticide and heavy-metal contaminants through the combined use of defect-engineered photoelectrodes, dual-photoelectrode amplification, and tuned interfacial charge-transfer routes. By merging light-driven energy conversion with selective interactions for molecular and ionic species, PBFC platforms attain strong sensitivity, tolerance to complex matrices, and stable operation, reinforcing their relevance for food-safety assessment and environmental monitoring in applied settings.

4.3. Toxin Detection

Toxins, including microcystins (MCs), aflatoxins, and patulin (PAT), pose persistent risks to food safety because they occur widely in aquatic and agricultural products and remain harmful at trace levels. In practice, toxin monitoring is challenged by low target abundance, fluctuating sample chemistry, and signal drift caused by matrix effects. PBFC-based self-powered sensors are well suited to this task because light-driven carrier generation enables bias-free operation and intrinsic amplification, while recognition layers translate toxin binding into controlled modulation of interfacial charge transfer. Recent progress can be organized around two recurring design logics: dual-photoelectrode energetic coupling for output amplification, and ratiometric or multiplexed signal management for robustness in real matrices.

A first design route strengthens cyanotoxin sensing by distributing functions across a dual-photoelectrode PBFC so that carrier separation, transport, and consumption are co-optimized at the system level. [105]. Building on the same principle, a PFC aptasensor integrating an In_2O_3-$CaIn_2S_4$/ITO photoanode with a $CuBi_2O_4$-PbS/ITO photocathode leveraged stepped band alignment and a Z-scheme photocathodic pathway to enhance interfacial charge transfer, thereby increasing usable output and enabling MC-LR quantification over a broad working window with reliable stability [106]. A conceptually aligned but cost-conscious configuration combined a TiO_2 photoanode with a nitrogen-doped graphene-BiOBr photocathode, and impedance analysis clarified that MC-LR oxidation primarily occurred at TiO_2 under illumination (Figure 8), providing a mechanistically explicit division of labor that supports rational dual-electrode optimization [107].

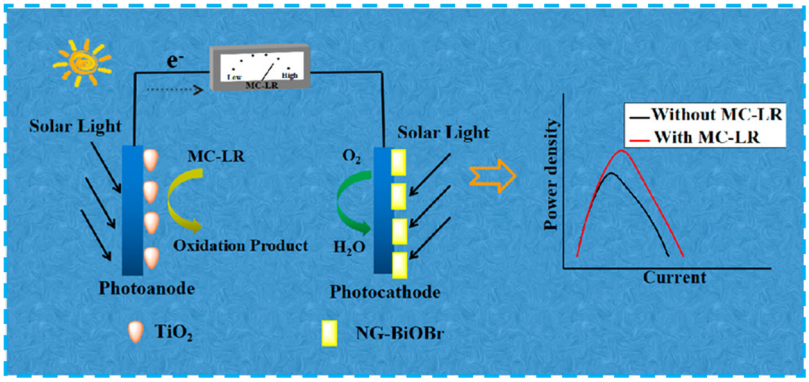

Figure 8. Schematic illustration of PEC for MC-LR detection. Reprinted with permission from Ref. [107]. Copyright, 2019, American Chemical Society.

A second route emphasizes system-level signal amplification and portability while retaining aptamer binding as the selectivity gate. A photo-driven self-powered aptasensor for MC-RR employed a $ZnIn_2S_4/Ti_3C_2$ heterojunction photoanode with a Cu_2O photocathode and integrated a matching capacitor to boost instantaneous output. In this design, Ti_3C_2 MXene promoted charge separation and provided a high surface area for aptamer immobilization, while capacitor matching converted transient current into a substantially amplified readout, enabling ultrasensitive signal-off detection via steric hindrance after target binding [108]. Importantly, the platform incorporated a USB-sized micro-workstation and a short-circuit current acquisition mode for real-time tracking, illustrating a practical pathway toward field-deployable cyanotoxin monitoring.

For mycotoxins, ratiometric and multichannel strategies are increasingly adopted to suppress drift arising from illumination fluctuations and instrumentation variability [109]. A ratiometric self-powered platform fabricated by laser direct writing used laser-induced CdS/TiO_2/graphene dual photoanodes addressed through multiplexed switching, and aptamer binding to aflatoxin B1 attenuated photocurrent via steric hindrance and hindered interfacial electron transfer. Quantification based on the ratio between a sensing channel and a reference channel reduced susceptibility to common-mode disturbances and improved reliability in real samples [110]. Complementarily, a portable multichannel photofuel cell chip with spatially resolved CdS/Bi_2S_3-modified photoanodes and a shared Prussian Blue cathode enabled ratiometric, simultaneous detection of OTA and PAT by using a control channel as an internal reference, providing a compact blueprint for multiplex toxin surveillance without external bias [111].

Overall, PBFC-based toxin sensing is advancing from single-electrode demonstrations toward systems in which dual-photoelectrode energetics provide amplification, and ratiometric or multichannel readouts provide robustness against matrix-induced drift. By aligning recognition chemistry with device-level carrier management, these platforms offer a coherent route to sensitive, portable, and interference-resilient toxin monitoring in food and environmental samples.

4.4. Integrated Functional Architectures

Practical deployment of PBFC sensors increasingly depends on whether energy transduction, signal readout, and interface regulation can be integrated into a self-consistent architecture, rather than optimized as separable modules [112]. A useful analogue is provided by implantable bioelectronics, where device function emerges from continuous coupling among optical, chemical, and electrical domains rather than from any single component in isolation. Shi et al. demonstrated that photoelectrochemical and electrochemical energy-conversion devices can regulate physiological activity via indirect, wireless energy transformation [113]. Silicon heterojunction membranes produced stable photocathodic currents under low-intensity illumination and enabled highly addressable multi-site cardiac pacing, whereas glucose- and lactate-powered biofuel cells supplied biocompatible outputs sufficient for local stimulation and metabolic sensing in physiological media. Together, these studies illustrate a continuously coordinated energy–signal network spanning optical, chemical, and electrical domains, offering a systems perspective that motivates PBFC food-safety sensors toward adaptive operation and feedback-like stability in chemically fluctuating matrices.

A complementary integration route embeds amplification within the electrode through chemistry-triggered electronic reconfiguration. Qin et al. reported an in situ defect-engineered WO_3 photoanode (E-WO_3) coupled to an enzymatic layer that locally generates ascorbic acid [114]. The resulting reductive microenvironment drives W^{6+} to W^{5+} conversion and oxygen-vacancy formation, narrowing the band gap and shifting the conduction-band edge; together, these changes enhance light absorption, reduce charge-transfer resistance, and stabilize photocurrent output. Functionally, the biochemical event reprograms the local electronic structure and acts as an internal amplification loop, enabling sensitive CEA quantification over a wide dynamic range.

Integration also determines usability at the device level, where portability and standardized acquisition define whether PBFC concepts translate beyond the laboratory. A visible-light-driven, self-powered PEC platform for real-time nodularin-R quantification combined a TiO_2-MXene photoanode interfaced with a handheld analyzer, enabling on-site operation under white LED illumination (Figure 9) [115]. The assembled system maintained stable 0 V-bias responses with low assay-to-assay variability and strong selectivity against coexisting biomolecules, and was reported to outperform conventional HPLC and ELISA in sensitivity and linear range under the tested conditions.

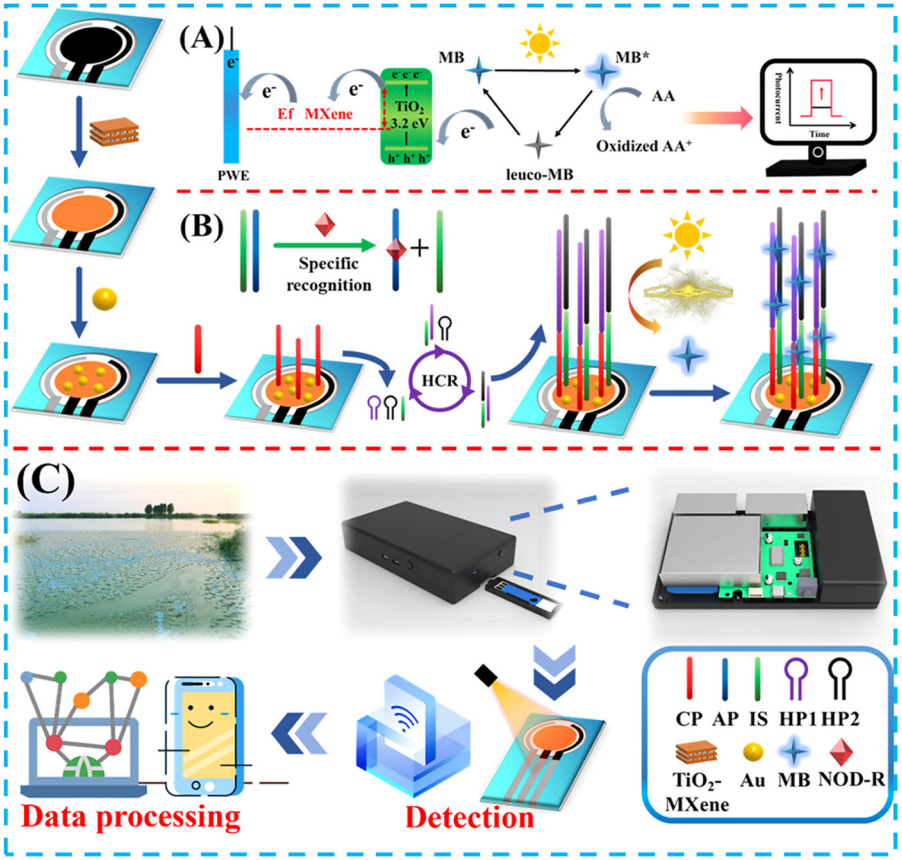

Figure 9. Schematic diagram of PEC sensing with TiO_2-MXene photoanode for nodularin-R detection. Reprinted with permission from Ref. [115]. Copyright 2024, American Chemical Society.

Overall, field-ready food monitoring requires PBFC architectures that tolerate heterogeneous media and recurrent perturbations in ionic strength, pH, and organic fouling [14,115,116]. Current trajectories therefore, favor integrated formats, including ratiometric dual-photoelectrode chips, microfluidic control of reaction microenvironments, and flexible battery-free packaging, all aimed at suppressing drift, stabilizing mass transport, and enabling reliable surveillance outside the laboratory.

5. Outlook and Perspectives

PBFC-based self-powered sensors are moving from proof-of-concept demonstrations toward field-relevant analytical platforms for distributed food-safety surveillance. Their key advantage lies in coupling light-driven carrier generation with catalytic redox turnover, thereby enabling bias-free signal output with inherent amplification in interference-prone matrices. However, translation remains limited by a small set of persistent bottlenecks: (i) photoelectrode degradation and interfacial drift under prolonged operation, (ii) modest energy-to-signal conversion efficiency under realistic mass-transport and fouling conditions, and (iii) incomplete system integration that prevents stable, standardized performance outside controlled settings. To overcome these limitations, a number of emerging strategies have been proposed. One effective approach involves the introduction of protective interlayers, such as metal oxide coatings deposited by atomic layer deposition, which can suppress photoelectrode corrosion by physically separating active components from aggressive electrolytes without sacrificing charge transport efficiency. In parallel, energy-to-signal conversion can be further improved through the construction of hierarchical heterostructures or the integration of plasmonic nanostructures, both of which broaden light absorption and promote interfacial redox dynamics. In addition, incorporating intrinsic calibration schemes, for example, ratiometric sensing based on dual signal outputs, provides a powerful means to minimize background interference and enhance analytical reliability [117].

In the future, the durability of materials and interfaces is likely to become a key factor for further development. In the matrix with high organic content, limiting interface pollution and controlling signal drift are crucial to maintaining selectivity during long-term operation. The progress of system integration and manufacturability will also affect the transformation of applications. The micro-flow control architecture can provide a stable micro-reaction environment and multiple detection functions that reduce sample consumption.

PBFC-specific indicators for stability, matrix tolerance, and repeatability will help to make meaningful comparisons. Integration with wireless communication and adaptive data analysis can also further provide drift correction, abnormal identification, and distributed monitoring functions in supply chain networks. Looking forward, PBFC-based sensing platforms are expected to progress toward more autonomous and adaptive sensing architectures. Rather than focusing solely on the performance of individual devices, future development will emphasize the integration of bioengineered recognition elements, such as genetically tailored enzymes or microbial systems, with flexible and conformable electronic substrates to enable wearable or packaging-embedded sensing formats. In parallel, advances in scalable fabrication technologies, including roll-to-roll processing, may facilitate large-area, low-cost production, allowing these sensors to function as distributed nodes within emerging food-monitoring networks. Such a paradigm shift could enable continuous, data-enabled assessment of food quality, supporting more accurate shelf-life management and improved transparency across supply chains [118].

Funding

This research was funded by the Open Project Funding of the Key Laboratory of Fermentation Engineering (Ministry of Education), Hubei University of Technology (No. 202409FE14).

Data Availability Statement

No novel data were generated.

Conflicts of Interest

The authors declare no conflict of interest.

Use of AI and AI-Assisted Technologies

During the preparation of this work, the authors used ChatGPT (version 5.2) to assist with language polishing. After using this tool/service, the authors reviewed and edited the content as needed and take full responsibility for the content of the published article.

References

1. Wang, P.-L.; Xie, L.-H.; Joseph, E.A.; et al. Metal-organic frameworks for food safety. *Chem. Rev.* **2019**, *119*, 10638.
2. Luo, X.; Zhao, J.; Li, M.; et al. Single-atom materials for food safety. *Mater. Today* **2023**, *64*, 121.
3. Kirby, R.; Teixeira, P. Consumer food trends and food safety: Challenges in modern food systems. *Trend. Food Sci. Tech.* **2025**, *166*, 105398.
4. Li, H.-R.; Xu, H.; Li, S.-S.; et al. Heterojunction composite-based electrochemical sensors for hazardous substances detection in environmental and biological system. *Coord. Chem. Rev.* **2025**, *540*, 216787.
5. Dashtian, K.; Shahbazi, S.; Tayebi, M.; et al. A review on metal-organic frameworks photoelectrochemistry: A headlight for future applications. *Coord. Chem. Rev.* **2021**, *445*, 214097.
6. Luo, X.; Tan, F.; Mao, Z.; et al. Single atom-bridged Au nanozymes boost glucose oxidase-like activity in acidic media. *Chem. Sci.* **2025**, *16*, 22160.
7. Yu, Z.; Tang, J.; Zeng, C.; et al. Shaping the future of the neurotransmitter sensor: Tailored CdS nanostructures for state-of-the-art self-powered photoelectrochemical devices. *ACS Sens.* **2024**, *9*, 2684.
8. Yu, Z.; Gong, H.; Li, Y.; et al. Chemiluminescence-derived self-powered photoelectrochemical immunoassay for detecting a low-abundance disease-related protein. *Anal. Chem.* **2021**, *93*, 13389.
9. Sun, X.; Chen, J.; Zhai, J.; et al. Beyond photosynthesis: $H_2O/H_2O_2/O_2$ self-circulation-based biohybrid photoelectrochemical cells for direct and sustainable solar-to-fuel-to-electric power conversion. *J. Am. Chem. Soc.* **2022**, *144*, 23073.
10. Luo, X.; Li, S.; Wu, Y.; et al. Hybrid enzymatic and nanozymatic biofuel cells for wearable and implantable biosensors. *TrAC Trend. Anal. Chem.* **2025**, *185*, 118169.
11. Gai, P.-P.; Ji, Y.-S.; Wang, W.-J.; et al. Ultrasensitive self-powered cytosensor. *Nano Energy* **2016**, *19*, 541.
12. Hao, S.; Sun, X.; Zhang, H.; et al. Recent development of biofuel cell based self-powered biosensors. *J. Mater. Chem. B* **2020**, *8*, 3393.
13. He, Y.; Chen, K.; Leung, M.K.H.; et al. Photocatalytic fuel cell-A review. *Chem. Eng. J.* **2022**, *428*, 131074.
14. Wang, L.; Zhang, J.-R.; Wu, X.; et al. Advances in the enzymatic biofuel cell powered sensing systems for tumor diagnosis and regulation. *TrAC Trend. Anal. Chem.* **2022**, *146*, 116476.

15. Sohel Rana, S.M.; Faruk, O.; Robiul Islam, M.; et al. Recent advances in metal-organic framework-based self-powered sensors: A promising energy harvesting technology. *Coord. Chem. Rev.* **2024**, *507*, 215741.
16. Theyagarajan, K.; Zahra, L.; Kim, Y.-J. Advances in the design and fabrication of flexible, wearable, and implantable electrochemical neurotransmitter sensors. *Coord. Chem. Rev.* **2026**, *549*, 217287.
17. Zhou, M. Recent Progress on the development of biofuel cells for self-powered electrochemical biosensing and logic biosensing: A review. *Electroanalysis* **2015**, *27*, 1786.
18. Wu, F.; Yu, P.; Mao, L. Self-powered electrochemical systems as neurochemical sensors: Toward self-triggered in vivo analysis of brain chemistry. *Chem. Soc. Rev.* **2017**, *46*, 2692.
19. Li, J.; Xu, C.; Shen, Y.; et al. A flexible electrochemical sensor for bisphenol A detection based on photoinitiated molecular imprinting on CdS functionalized carbon felt. *Anal. Chim. Acta* **2023**, *1281*, 341923.
20. He, Y.; Sun, J.; Yao, W.; et al. A self-powered photoelectrochemical molecular imprinted sensor for chloroquine phosphate with enhanced cathodic photocurrent via stepped energy band alignment engineering. *Chem. Eng. J.* **2023**, *451*, 138748.
21. Majani, S.S.; Basavaraj, R.B.; Sureshkumar, K.; et al. Photo-accelerated detoxification of Norfloxacin and electrochemical sensing application of engineered deep orange-red emitting samarium doped $SrCeO_3$ nanostructures. *Mater. Today Adv.* **2025**, *28*, 100634.
22. Jiang, J.; Wu, T.; Wei, M.; et al. Self-powered photoelectrochemical sensing for sensitive detection of chloramphenicol based on sulfur-vacancy engineered MoS_2 nanoribbons/plasmonic Ti_3C_2 MXene with continual injection of photoinduced electrons. *J. Environ. Chem. Eng.* **2024**, *12*, 112067.
23. Dashtian, K.; Hajati, S.; Karimi, R.; et al. Near-infrared-responsive photoelectrochemical biosensors. *TrAC Trend. Anal. Chem.* **2024**, *179*, 117890.
24. Xu, X.; Zhou, X.; Huang, J.; et al. High-throughput multitarget molecular detection in an automatic light-addressable photoelectrochemical sensing platform. *Anal. Chem.* **2024**, *96*, 9185.
25. Le, P.G.; Kim, M.I. Research progress and prospects of nanozyme-based glucose biofuel cells. *Nanomaterials* **2021**, *11*, 2116.
26. Chen, Y.; Ji, W.; Yan, K.; et al. Fuel cell-based self-powered electrochemical sensors for biochemical detection. *Nano Energy* **2019**, *61*, 173.
27. Toe, C.Y.; Zhou, S.; Gunawan, M.; et al. Recent advances and the design criteria of metal sulfide photocathodes and photoanodes for photoelectrocatalysis. *J. Mater. Chem. A* **2021**, *9*, 20277.
28. Zhou, S.; Jiang, C.; Han, J.; et al. High-performance self-powered PEC photodetectors based on 2D $BiVO_4$/MXene schottky junction. *Adv. Funct. Mater.* **2024**, *35*, 2416922.
29. Zhou, S.; Liu, X.; Gunawan, M.; et al. Unassisted photoelectrochemical hydrogen production coupled with selective glucose oxidation using metal halide perovskite photoanodes. *Adv. Funct. Mater.* **2025**. https://doi.org/10.1002/adfm.202505281.
30. Sui, Q.; Li, H.; Xia, J.; et al. Unbiased photoelectrochemical H_2O_2 production using boron nitride for both photogenerated hole extraction and oxygen reduction selectivity regulation. *Angew. Chem. Int. Ed.* **2025**, *64*, e202520190.
31. Ma, N.; Lu, C.; Liu, Y.; et al. Direct Z-scheme heterostructure of vertically oriented SnS_2 nanosheet on $BiVO_4$ nanoflower for self-powered photodetectors and water splitting. *Small* **2024**, *20*, e2304839.
32. Jiang, F.; Liu, S.; Dong, H.; et al. Self-powered photoelectrochemical immunosensor with triple enhanced photoelectric response for sensitive detection of cTnI. *Sens. Actuators B Chem.* **2023**, *393*, 134234.
33. Zheng, Q.; Tang, Q.; Wang, Z.L.; et al. Self-powered cardiovascular electronic devices and systems. *Nat. Rev. Cardiol.* **2021**, *18*, 7.
34. Cestellos-Blanco, S.; Zhang, H.; Kim, J.M.; et al. Photosynthetic semiconductor biohybrids for solar-driven biocatalysis. *Nat. Catal.* **2020**, *3*, 245.
35. Shen, F.; Xiao, X.; Dai, Q.; et al. Combining enzymatic biofuel cells with supercapacitors to self-charging hybrid devices. *Chem. Rec.* **2025**, *25*, e202400248.
36. Kim, S.; Kim, M.; Kim, H. Self-powered photodetectors based on two-dimensional van der Waals semiconductors. *Nano Energy* **2024**, *127*, 109725.
37. Wang, L.; He, G.; Wang, H.; et al. A self-powered photoelectrochemical sensing array based on Ni-doped Co_3O_4 photocathode for high-throughput detection of environmental pollutant dibutyl phthalate. *Sens. Actuators B Chem.* **2025**, *445*, 138568.
38. King, A.J.; Weber, A.Z.; Bell, A.T. Understanding photovoltage enhancement in metal-insulator semiconductor photoelectrodes with Metal Nanoparticles. *ACS Appl. Mater. Inter.* **2024**, *16*, 36380.
39. Wang, Q.; Niu, X.; Ning, W.; et al. Interaction of organic-inorganic hybrid perovskite electron system with lattice system. *Mater. Today Sust.* **2024**, *25*, 100617.
40. Zhang, Y.; Liu, J.; Singh, M.; et al. Superionic conductivity in ceria-based heterostructure composites for low-temperature solid oxide fuel cells. *Nano-micro lett.* **2020**, *12*, 178.
41. Dai, M.; He, Z.; Zhang, P.; et al. $ZnWO_4$-$ZnIn_2S_4$ S-scheme heterojunction for enhanced photocatalytic H_2 evolution. *J. Mater. Sci. Technol.* **2022**, *122*, 231.

42. Dou, L.; Lu, D.; Guo, H.; et al. Novel self-powered anti-interference photoelectrochemical sensor via zirconium porphyrin-based metal-organic framework as multifunctional signal label for oxytetracycline detection in food and environment. *Chem. Eng. J.* **2024**, *496*, 153979.
43. Wang, Y.; Zhang, A.; Liu, J.; et al. Mosaic Se/InSe heterojunction for self-powered bipolar photodetection. *Adv. Opt. Mater.* **2023**, *12*, 2302149.
44. Zhang, N.; Gao, X.; Guan, H.; et al. Three-dimensional porous In_2O_3 arrays for self-powered transparent solar-blind photodetectors with high responsivity and excellent spectral selectivity. *Nano Res.* **2023**, *17*, 4471.
45. Dong, R.; Wang, H.; Zhang, J.; et al. Self-powered SiC-based photoelectrochemical ultraviolet photodetectors for robust underwater optical communication against full aquatic environments. *Adv. Sci.* **2026**, *13*, e13939. https://doi.org/10.1002/advs.202513939e13939.
46. Song, H.; Liu, J.; Wu, Y.; et al. High-performance dual-band self-powered photoelectrochemical photodetector based on type-I In_2Te_3/Se heterostructure for encrypted optical communication. *Nano Lett.* **2025**, *25*, 11689.
47. Jiang, D.; Cao, X.; Shi, Y.; et al. Flexible $Ti_3C_2T_x$ MXene Regulated Photoelectrochemical Sensing Platform for Sensitive Monitoring of Dopamine. *Adv. Funct. Mater.* **2025**, *34*, 2410546.
48. Azadmanjiri, J.; Regner, J.; Děkanovský, L.; et al. Powering the future: Unleashing the potential of MXene-based dual-functional photoactive cathodes in photo-rechargeable Zinc-ion capacitor. *Small* **2024**, *20*, 2305972.
49. Jahangir, T.N.; Kandiel, T.A.; Mahar, N.; et al. Exploring the role of $Ti_3C_2T_x$MXene in photoelectrochemical water splitting over solution-processed $BiVO_4$ photoanode. *Mater. Today Energy* **2024**, *40*, 101469.
50. Chen, Z.; Liao, Y.; Chong, H.; et al. The CoNi@C/$Mo_{1.33}$C i-MXene derived from novel $(Mo_{2/3}R_{1/3})_2GaC$ (R = Dy, Ho, Er, Tm, and Lu) nanolaminations for electrochemical application in electrocatalytic hydrogen evolution and supercapacitance. *Small* **2025**, *21*, 2407667.
51. Dang, C.; He, S.; Liu, Y.; et al. Designing In_2S_3@Bi_2S_3 type II heterostructure for bifunctional photo-enhanced Li-O_2 batteries. *Chem. Eng. J.* **2023**, *476*, 146775.
52. Li, L.; Bo, Y.; Miao, P.; et al. Self-powered photoelectrochemical immunosensing platform for sensitive CEA detection using dual-photoelectrode synergistic signal amplification. *Biosens. Bioelectron.* **2024**, *250*, 116075.
53. Liu, S.; Dong, H.; Jiang, F.; et al. Wang, J. Self-powered photoelectrochemical biosensor with inherent potential for charge carriers drive. *Biosens. Bioelectron.* **2022**, *211*, 114361.
54. Jeerapan, I.; Sempionatto, J.R.; Wang, J. On-body bioelectronics: Wearable biofuel cells for bioenergy harvesting and self-powered biosensing. *Adv. Funct. Mater.* **2020**, *30*, 1906243.
55. Song, L.; Fan, Y.; Fan, H.; et al. Photo-assisted rechargeable metal batteries. *Nano Energy* **2024**, *125*, 109538.
56. Wang, W.; Zhang, X.; Lin, J.; et al. A Photoresponsive battery based on a redox-coupled covalent-organic-framework hybrid photoelectrochemical cathode. *Angew. Chem. Int. Ed.* **2022**, *61*, e202214816.
57. Jing, L.; Xu, Y.; Xie, M.; et al. Piezo-photocatalysts in the field of energy and environment: Designs, applications, and prospects. *Nano Energy* **2023**, *112*, 108508.
58. Chae, S.Y.; Mehmood, A.; Park, E.D. Photoelectrochemical tandem chlorination of sp^3 C-H bond in seawater/chloroform two-phase electrolyte system by Ti-doped Fe_2O_3 photoanode. *J. Am. Chem. Soc.* **2025**, *147*, 19472
59. Zhu, K.; Zhang, X.; Wen, L.; et al. Electrochemical formation of $BiVO_4$/$BiPO_4$ photoanodes for enhanced selectivity toward H_2O_2 generation. *Adv. Funct. Mater.* **2025**. https://doi.org/10.1002/adfm.202517929.
60. Sun, S.; Li, W.; Zhang, Y.; et al. Mixed metal oxide heterojunction for high-performance self-powered ultraviolet photodetection. *Small* **2024**, *21*, e2407107.
61. Miao, Y.; Li, Z.; Luo, L.; et al. Photoelectrocatalytic allylic C-H oxidation to allylic alcohols coupled with hydrogen evolution. *Appl. Catal. B Environ.* **2025**, *361*, 124588.
62. Dong, Y.; Guo, C.; Zheng, R.; et al. Synergistic signal amplification by Cu_2O-Au/Ag nanozyme in heterojunction photoanode for high-sensitivity photoelectrochemical detection of Cyfra21-1. *Small* **2025**, *21*, e02779.
63. Wang, M.; Yan, Z.; Yun, Q.; et al. Self-powered broadband underwater optical communication enabled by enhanced donor-acceptor molecular junction in π-conjugated covalent organic framework. *Chem. Eng. J.* **2025**, *524*, 169368.
64. Xiao, K.; Zhu, R.; Du, C.; et al. Zinc-air battery-assisted self-powered PEC sensors for sensitive assay of PTP1B activity based on perovskite quantum dots encapsulated in vinyl-functionalized covalent organic frameworks. *Anal. Chem.* **2022**, *94*, 9844.
65. Pu, Y.; Zhu, S.; Chang, Y.; et al. CoAl layered double hydroxides decorated $BiVO_4$ photoanode for highly efficient removal of antibiotics in photoelectrochemical-chloride system. *Chem. Eng. J.* **2025**, *519*, 165246.
66. Chen, S.; Liu, Y.; Wu, J.; et al. Dimension-controlled BC_2N nanoarchitectures: A novel strategy for superior photoelectrochemical photodetection performance. *Chem. Eng. J.* **2025**, *520*, 165599.
67. Chen, Y.; Zhang, X.; Liu, Y.; et al. Gold nanoparticles and MXene nanocomposite based electrochemical sensor for point-of-care monitoring of serum biomarkers. *ACS Nano* **2025**, *19*, 16980.

68. Ye, Q.; Chen, H.; Yao, R.; et al. Self-powered photoelectrochemical solar-blind UV photodetector with enhanced responsivity SnO_2 nanosheets-$Ti_3C_2T_x$. *Surf. Inter.* **2024**, *52*, 104851.
69. Shi, Y.; Song, G.; Yang, B.; et al. Prussian blue analogues "dressed" in MXene nanosheets tightly for high performance lithium-ion batteries. *Adv. Mater.* **2025**, *37*, e2416665.
70. Li, H.J.; Huang, C.; Wang, F.; et al. Photo-nanozyme-integrated photoelectrochemical-electrochemical dual-mode biosensor: Enabling amplification-free detection of miRNA-133a in acute myocardial infarction. *Anal. Chem.* **2025**, *97*, 6686.
71. Xiao, Z.; Chen, Y.; Zhang, Y. Self-powered portable photoelectrochemical sensor based on dual-photoelectrode for microplastics detection. *Environ. Res.* **2025**, *271*, 121084.
72. Wang, D.; Ding, Z.; Cheng, H.; et al. High-performance self-powered photoelectrochemical bioassay system with a triphase oxidase enzymatic interface. *Sens. Actuators B Chem.* **2023**, *392*, 134125.
73. Li, J.; Liu, C.; Dang, C.; et al. Light-switched electron migration routes via Co-catecholates grafted on Z-scheme Cu_2O@CuO heterostructure for photoelectrochemical hydrogen evolution. *Chem. Eng. J.* **2025**, *505*, 159864.
74. Cai, Q.; Li, H.; Li, Z.; et al. Single-atom iron boosts interfacial oxygen reduction for self-powered photoelectrochemical biosensing. *Anal. Chem.* **2025**, *97*, 17580.
75. Tan, R.; Qin, Y.; Liu, M.; et al. Bifunctional single-atom iron cocatalysts enable an efficient photoelectrochemical fuel cell for sensitive biosensing. *Adv. Funct. Mater.* **2023**, *33*, 2305673.
76. Tian, S.; Yu, Z.; Wang, Y.; et al. Crystal facet engineering modulated electron transfer mechanisms: A self-powered photoelectrochemical sensing platform for noninvasive detection of uric acid. *Anal. Chem.* **2025**, *97*, 9518.
77. Song, X.; Ming, Y.; Liu, J.; et al. Highly catalytic CoFe-prussian blue analogue/ZIF-67 yolk-shell nanocube-decorated MBene nanosheets for ultrasensitive electrochemical cancer-specific neoantigen biosensor. *J. Colloid Interface Sci.* **2025**, *683*, 58.
78. Guo, X.; Zhang, H.; Wang, Y.; et al. Confining asymmetrically coordinated cobalt single-atoms/clusters on holey MXene for ultrafast fenton-like catalysis. *Angew. Chem. Int. Ed.* **2025**, *64*, e202511266.
79. Leng, D.; Ren, X.; Liu, L.; et al. A self-powered photoelectrochemical biosensing platform for H-FABP monitoring mediated by $CsPbBr_3$@COF-V. *Biosens. Bioelectron.* **2023**, *241*, 115710.
80. Li, Y.; Cheng, F.; Qi, Y.; et al. Synthesis of Ti_2CO_2 MXene and its application in photoelectrochemical biosensors with ultrahigh sensitivity and long-term stability. *ACS Nano* **2025**, *19*, 22007.
81. Liu, B.; Ge, Y.; Lu, Y.; et al. An NIR light-responsive "on-off-on" photoelectrochemical aptasensor for carcinoembryonic antigen assay based on Y-shaped DNA. *Biosens. Bioelectron.* **2023**, *229*, 115241.
82. Ban, R.; Lu, M.J.; Hu, J.; et al. Biological modulating organic photoelectrochemical transistor through in situ enzymatic engineering of photoactive gate for sensitive detection of serum alkaline phosphatase. *Biosens. Bioelectron.* **2022**, *218*, 114752.
83. Wang, J.; Kong, J.; Zhang, X. Riboflavin-induced photo-ATRP electrochemical strategy for detection of biomarker trypsin. *Talanta* **2024**, *277*, 126386.
84. Niu, X.; Zheng, N.; Liao, M.; et al. $Cu_{x+1}O$-mediated photo-nanozyme-integrated photoelectrochemical-colorimetric dual-readout biosensing for sensitive detection of MiRNA. *Sens. Actuators B Chem.* **2025**, *444*, 138383.
85. Tian, T.; Song, D.; Zhen, L.; et al. Colorimetric-Fluorescence-Photothermal tri-mode sensor array combining the machine learning method for the selective identification of sulfonylurea pesticides. *Biosens. Bioelectron.* **2025**, *277*, 117286.
86. Fang, Y.; Hao, L.L.; Xiao, J.Y.; et al. Photo-manipulating the interlayer spacing of MXene toward switchable electrochemical and gas sensing functionality. *Adv. Funct. Mater.* **2025**, *35*, 2421833.
87. Cao, D.; Wu, W.; Fang, J.; et al. Dual-mode self-powered photoelectrochemical and colorimetric determination of procalcitonin accomplished by multienzyme-expressed Ni_4Cu_2 bimetallic hollow nanospheres and spherical nanoflower-MoS_2/Cu_2ZnSnS_4/Bi_2S_3. *Anal. Chim. Acta* **2024**, *1288*, 342056.
88. Wang, H.; Zhang, T.; Chen, X.; et al. Colorimetric-assisted photoelectrochemical sensing for dual-mode detection of neuron-specific enolase via the photoanode-photocathode system. *Anal. Chem.* **2025**, *97*, 15350.
89. Luo, G.; Sun, Y.; Du, C.; et al. Self-powered PEC platform with large and stable photocurrent for blocker-free sensitive assay of Caspase-3 activity based on $CdIn_2S_4$/CdS QDs anode and NH_2-MIL-125Ti@$MAPbI_3$/Au NPs cathode. *Biosens. Bioelectron.* **2025**, *278*, 117350.
90. Liu, J.; Lv, L.; Leng, D.; et al. Interface self-shelling effect-mediated photoinduced carrier transport and multiplexed signal amplification mechanism in self-powered photoelectrochemical biosensing. *Biosens. Bioelectron.* **2025**, *284*, 117577.
91. Parvulescu, V.I.; Epron, F.; Garcia, H.; et al. Recent progress and prospects in catalytic water treatment. *Chem. Rev.* **2022**, *122*, 2981.
92. Zhu, L.; He, Y.; Huang, H.; et al. Synergistic enhancement of PEC activity in heterojunction assisted by oxygen vacancies and ferroelectric polarization at zero bias: Mechanism study and achievement of ultrasensitive detection. *Anal. Chem.* **2025**, *97*, 4166.

93. Yang, P.; Jiang, H.; Zhang, H.; et al. Synergistic signal amplification-initiated innovative self-powered photoelectrochemical aptasensing: An ingenious photocathode activated by the high-light-harvesting photoanode. *Anal. Chem.* **2023**, *95*, 7303.
94. Lu, K.; Hong, C.; Liu, D.; et al. A self-powered molecular imprinted photoelectrochemical sensor for streptomycin cathodic detection based on a signal amplification of ZnO/ZnS/Ag_2S photoanode. *Sens. Actuators B Chem.* **2022**, *371*, 132588.
95. Leng, D.; Song, L.; Du, Y.; et al. Advancing microfluidic photoelectrochemical aptasensing platform with photogenerated carrier regulation for protein biosynthesis inhibitors detection. *Anal. Chem.* **2025**, *97*, 17788.
96. Fan, X.; Peng, J.; Zhang, X.; et al. Reconfiguration/immobilization "dual-free" self-powered multiplex photoelectrochemical strategy for dual magnetic bead-mediated dimension differentiate type complex sample assay. *Anal. Chem.* **2025**, *97*, 11778.
97. Tang, J.; Bai, X.; Ji, Y.; et al. Signal amplified self-powered cathodic photoelectrochemical sensor based on elevating potential strategy and prolonging electron lifetime. *Sens. Actuators B Chem.* **2025**, *426*, 137108.
98. Hu, S.; Wei, Y.; Wang, J.; et al. A photo-renewable ZIF-8 photo-electrochemical sensor for the sensitive detection of sulfamethoxazole antibiotic. *Anal. Chim. Acta* **2021**, *1178*, 338793.
99. Zhang, L.; Zhang, Y.; Chen, W.-T.; et al. Recent advances and perspectives in functionalized nanocomposites for electrochemical sensing of toxic environmental heavy metal ions. *Coord. Chem. Rev.* **2025**, *542*, 216859.
100. Guo, A.; Song, M.; Chen, Q.; et al. Enhanced label-free photoelectrochemical strategy for pollutant detection: Using surface oxygen vacancies-enriched $BiVO_4$ photoanode. *Anal. Chem.* **2024**, *96*, 9944.
101. Chen, S.; Lan, W.; Yang, D.; et al. Self-powered photoelectrochemical sensor based on molecularly imprinted polymer-coupled CBFO photocathode and Ag_2S/SnS_2 photoanode for ultrasensitive dimethoate sensing. *Anal. Chim. Acta* **2025**, *1337*, 343556.
102. Du, X.; Du, W.; Sun, J.; et al. Self-powered photoelectrochemical sensor for chlorpyrifos detection in fruit and vegetables based on metal-ligand charge transfer effect by Ti_3C_2 based Schottky junction. *Food. Chem.* **2022**, *385*, 132731.
103. Hu, J.; Li, Z.; Zhai, C.; et al. Photo-assisted simultaneous electrochemical detection of multiple heavy metal ions with a metal-free carbon black anchored graphitic carbon nitride sensor. *Anal. Chim. Acta* **2021**, *1183*, 338951.
104. Zou, W.; Li, Q.; Wu, Q.; et al. Bifunctional Dy-MOF for efficient electrochemical detection and photocatalytic reduction of Cr(VI). *Chem. Eng. J.* **2025**, *505*, 159428.
105. Dai, H.; Zhang, S.; Wei, J.; et al. A self-powered photoelectrochemical aptasensing platform for microcystin-LR cathodic detection via integrating Bi_2S_3 photoanode and $CuInS_2$ photocathode. *Sens. Actuators B Chem.* **2023**, *397*, 134692.
106. Wang, Y.; Wang, Y.; Wang, L.; et al. A self-powered PFC sensing platform via integrating aptamer-modified photoanode and Z-scheme signal amplifying photocathode for microcystin-LR detection. *Anal. Chim. Acta* **2025**, *1347*, 343792.
107. Du, X.; Jiang, D.; Liu, Q.; et al. Ingenious dual-photoelectrode internal-driven self-powered sensing platform for the power generation and simultaneous microcystin monitoring based on the membrane/mediator-free photofuel cell. *Anal. Chem.* **2019**, *91*, 1728.
108. Sun, J.; Zhu, R.; Du, X.; et al. An ultrasensitive photo-driven self-powered aptasensor for microcystin-RR assay based on $ZnIn_2S_4/Ti_3C_2$ MXenes integrated with a matching capacitor for multiple signal amplification. *Analyst* **2023**, *148*, 5060.
109. Wei, J.; Hu, Q.; Gao, Y.; et al. A multiplexed self-powered dual-photoelectrode biosensor for detecting dual analytes based on an electron-transfer-regulated conversion strategy. *Anal. Chem.* **2021**, *93*, 6214.
110. Qiu, Z.; Yang, Y.; Xue, X.; et al. Laser-induced CdS/TiO_2/graphene dual photoanodes for ratiometric self-powered photoelectrochemical sensor: An innovative approach for aflatoxin B1 detection. *Microchim. Acta* **2024**, *191*, 630.
111. Yan, K.; Ding, Y.; Liu, X.; et al. Portable self-powered electrochemical aptasensing platform for ratiometric detection of mycotoxins based on multichannel photofuel cell. *Anal. Chim. Acta* **2024**, *1299*, 342442.
112. Chang, Z.; Wang, F.; Wang, Z.; et al. Fiber-based electrochemical sweat sensors toward personalized monitoring. *Prog. Mater. Sci.* **2026**, *156*, 101579.
113. Shi, J.; Li, P.; Kim, S.; et al. Implantable bioelectronic devices for photoelectrochemical and electrochemical modulation of cells and tissues. *Nat. Rev. Bioeng.* **2025**, *3*, 485.
114. Qin, J.; Yu, Z.; Wu, D.; et al. Target-induced oxygen vacancy on the etching WO_3 photoanode for in-situ amplified photoelectrochemical immunoassay. *Biosens. Bioelectron.* **2025**, *279*, 117405.
115. Dai, H.; Ahmad, W.; Zhang, S.; et al. A visible-light-driven self-powered nodularin-R biosensing platform controlled by an integrated portable photoelectrochemical detection device. *Anal. Chem.* **2024**, *96*, 12526.
116. Lei, W.; Zhang, S.; Shu, J.; et al. Self-powered glucose biosensor based on non-enzymatic biofuel cells by Au nanocluster/Pd nanocube heterostructure and Fe_3C@C-Fe single-atom catalyst. *Small* **2025**, *21*, e2410326.
117. Bae, S.; Moehl, T.; Service, E.; et al. A hole-selective hybrid TiO_2 layer for stable and low-cost photoanodes in solar water oxidation. *Nat. Commun.* **2024**, *15*, 9439.
118. Li, W.; Wen, J.; Gu, W.; et al. Recent advances in signal amplification strategies for photoelectrochemical sensing. *J. Anal. Test.* **2025**, *93*, 13389–13397. https://doi.org/10.1007/s41664-025-00417-3.